

Vortex Arrays of Coexisting Single and Double-Quantum Vortex Lines in $^3\text{He-A}$ U. Parts^a, V.V. Avilov^b, J.H. Kojivunen^a, N.B. Koprin^{a,c}, M.Krusius^a, J.J. Ruohio^a, and V.M.H. Ruutu^a^aLow Temperature Laboratory, Helsinki University of Technology, P.O.Box 2200, FIN-02015 HUT, Finland^bDepartment Magnetohydrodynamics Research Center Rossendorf, P.O.Box 510119, D-01314 Dresden, Germany^cL.D. Landau Institute for Theoretical Physics, 117334 Moscow, Russia

(May 19, 2019)

In superfluid $^3\text{He-A}$ singly and doubly quantized vortex lines can coexist in a rotating container. Using cw NMR we identify the external variables which control their coexistence and record the radial distribution in which the two species appear in a vortex array. The distribution is found to depend on the procedure by which the array is prepared. Two methods of preparation have been found. By comparison with numerical simulation we conclude that in one case a glassy agglomeration is formed. This shows that in superfluid ^3He the energy barriers separating different configurations of the vortex array are impenetrably high for metastabilities to anneal. In the second case the vortices and the array are formed simultaneously on cooling through T_c in rotation. Here the two vortex species are found to segregate into two coaxial domains.

PACS: 67.57.Fg, 52.25.Wz, 74.60.Ge

I. INTRODUCTION

Superfluid $^3\text{He-A}$ is the only known system where topologically stable vortex lines with different quantization can appear simultaneously. The doubly quantized vortex (DQV) is formed at low critical velocity and is usually obtained when superfluid $^3\text{He-A}$ is accelerated to motion, e.g. in a rotating container [1]. The singly quantized vortex (SQV), in turn, may have lower energy, depending on the magnitude of the magnetic field and flow velocity, but because of its large critical velocity it is in practice only formed on cooling through the superfluid transition in nonzero flow [2]. Normally one will thus find either double or single-quantum vortex lines in a rotating container, depending on how the state has been prepared.

In the homogeneous rotating superfluid, transitions between different vortex textures are of first order and sharp. Topological stability forbids a transition from one type of existing vortex lines to another. Thus SQV and DQV lines, once they have been formed, will maintain their quantization in the rotating container, as long as they are not removed by deceleration and annihilation on the container wall or by warming up to the normal phase. In principle, one can prepare a rotating state where both types of vortex lines are simultaneously present. A priori it is not clear what configuration a rotating state with two different vortex species would take: Do the arrays always have the same configuration or does this depend on the process by which the state has been created? Similar questions have been studied in the case of point-like objects, namely trapped ions in a 2 or 3-dimensional point charge system (see e.g. [3]).

In the present paper we address the problem of coexisting SQV and DQV both theoretically and experimentally. We investigate free energies of various configurations of vortex arrays consisting of separate SQV and DQV, as well as mixtures of these two types of vor-

tices. We apply both the continuum model and use the numerical simulations of discrete vortex arrays to show that the configurations with SQV vortices surrounding the inner cluster of DQV have lower energies as compared to any other configuration. The energy difference is very small and disappears in the continuum approximation. Experimentally, we find axial configurations with coexisting SQV and DQV lines when a cylindrical rotating container filled with liquid ^3He is slowly cooled from the normal to the superfluid A phase. Our observations for such states agree with the theoretical predictions based on the energy minimization: the SQV lines are found in outer regions of the cylinder while DQV occupy the inner regions of the vortex cluster. Non-axial segregated configurations can also be prepared when the container is accelerated at a constant temperature from a rotating state which had initially only the SQV lines. These configurations do not correspond to the global energy minimum but rather resemble glassy agglomerates.

II. ROTATING $^3\text{He-A}$.

Rotating vortex states are driven by superfluid counterflow (CF), the difference in the velocities of the normal and superfluid fractions, $v = v_n - v_s$. The equilibrium states are found by minimizing the free energy functional [4], which controls the spatial distribution of the orientation of the order parameter. On a scale of one vortex unit cell, accurate numerical minimization of the free energy have been performed for the homogeneous case in an infinite superfluid bath with periodic boundary conditions as a function of the rotation velocity and the applied field H [5,2,6]. These calculations reveal a complex phase diagram [2,6], with quantized vorticity organized in many, both topologically and structurally, different types of periodic order parameter textures of the spin $\hat{\mathbf{d}}(\mathbf{r})$ and or-

bital $\hat{\mathbf{l}}(\mathbf{r})$ vector fields [7]. Singular vortex textures have only been described approximately, by solving for the order parameter distribution with analytical trial functions [8].

On a macroscopic scale, vortex textures in $^3\text{He-A}$ are rectilinear structures, oriented parallel to the rotation axis. In the rotating container they extend from the top to the bottom of the cylinder. The existing vortex cells are confined by the Magnus force to a regular array, a cluster of vortex lines, which is located coaxially along the axis of the cylinder [9]. The cluster is isolated from the cylindrical wall by an annular layer of vortex-free CF. Within the cluster the areal density of linear vortex cells has the solid-body-rotation value $n = 2 = \frac{1}{2} \pi \rho_0$. Here $\rho_0 = \frac{I}{2\pi}$ is the circulation of a vortex line with the quantum number ℓ and the circulation quantum $h = \hbar(2m_3) = 0.0667 \text{ m m}^2/\text{s}$. In a vortex cluster of infinite diameter a transverse cross section would display a 2-dimensional array with triangular nearest-neighbor coordination, which arises from the inter-vortex repulsion. In a finite cluster the central region is also expected to exhibit triangular coordination, with almost crystalline order. The outer boundary of the cluster, in contrast, is deformed by the surrounding annular CF to a circle. Thus on moving out from the center the array deforms more and more towards a con guration of concentric rings of vortex lines. Due to this competition between volume and surface interactions long range order is relatively poor in finite-size arrays [10] at the usually experimentally accessible rotation velocities. Here the total number of lines is typically a few hundred, the radius of the container R a few mm, the radius of the Wigner-Seitz (WZ) cell of the vortex lattice $r_0 \approx 100 \text{ m}$, and the vortex core radius $c \approx 10 \text{ m}$.

In an array consisting of DQV lines the intervortex distance is larger by $\sqrt{2}$ than in one formed from SQV lines. With coexisting SQV and DQV lines the large difference in the cross sectional size of the two vortex species opens the question whether it creates sufficient mismatch and distortion in the nearest-neighbor coordination that a disordered glassy state results. Or it could lead to a "chemical" structure where both species occupy fixed positions within a periodically repeating unit cell. A third possibility is an array consisting of segregated domains of one species only.

III. ENERGY INTEGRATION

A. Continuous approximation

We start our study of various vortex configurations with the energy argumentation. The fine structure of the vortex line in the transition regime with two competing species is governed by smaller energy contributions, on the order of the spin-orbit energy. A larger source of

the energy difference between SQV and DQV arrays is provided on a macroscopic level by the difference in the quantization numbers and in the intervortex distances if the latter are much longer than the soft core size. We concentrate on the kinetic energy of superflow neglecting the smaller energy associated with the structure of the soft vortex core.

Consider the free energy of a rotating superfluid

$$E_{\text{fvsg}} = E_{\text{kin}} - \frac{s}{2} \int_{r < R} (v_s^2 - 2v_s v_{\text{rot}}) d^2 r ; \quad (1)$$

where $v_{\text{rot}} = \frac{1}{2} \omega r$. It should be minimized for given s , where L is the angular momentum of the fluid. We use first the continuum approximation for the superflow velocity and assume the logarithmic expression for the vortex energy. In the laboratory frame we have (compare with Ref. [11])

$$E = \frac{s}{2} \int_0^R v_s^2 + \frac{|\text{curl } v_s|_z}{2} \ln \frac{r_0}{2v_s r} - d^2 r. \quad (2)$$

The second term in the integral introduces the energy of a vortex line. If several vortex species are present, $s = s_0, r_0$, and v_s are functions of the spatial coordinates. Eq. (2) does not include the surface energies at the interfaces between the vortex cluster and the vortex-free region or between the segregated regions occupied by different vortex species. Nor does it account for interactions between the vortex lines and the container walls. The average velocity field is $v_s = v_{s0}$ where

$$v_{s0} = \begin{cases} v_{\text{rot}}; & \text{if } r < R_v \\ [\frac{1}{2} \omega r] R_v^2 = r^2; & \text{if } r > R_v \end{cases} \quad (3)$$

Here R_v is the radius of the entire vortex cluster in the coaxial configuration.

Let us assume that N_a vortices of type a with circulation ℓ_a , intervortex distance r_a , and core size c_a are in a central cluster, coaxial with the cylinder and with a radius R_a . The exterior region is filled with N_b vortices of type b with circulation ℓ_b , intervortex distance r_b , and core size c_b . We have

$$r_a^2 = \frac{a}{2}; \quad r_b^2 = \frac{b}{2}; \quad R_a^2 = \frac{N_a a}{2}; \quad (4)$$

so that

$$N_a a + N_b b = 2 R_v^2; \quad (5)$$

The overall radius $R_v(a;b)$ of the entire vortex cluster with vortices of type a in the center may be different from $R_v(b;a)$, when the vortices of type b are in the center. The energy in Eq. (2), with the a type of vortices in the center, is given by

$$\frac{E(a;b)}{E_0} = \frac{R_v}{R} \left(\frac{3}{4} \ln \frac{R_v}{R} + \frac{R_v}{R} \right)^2 + b \frac{R_v}{R}^2 + (a-b) \frac{R_a}{R}^2 ; \quad (6)$$

where $E_0 = \frac{1}{2} R^2 \ln \frac{R^2}{R_a^2}$. The normalized vortex energies in the logarithm is approximation (see Eq.(18)) are

$$b = \frac{R_b^2}{R^2} \ln \frac{R_b}{e_b} ; \quad a = \frac{R_a^2}{R^2} \ln \frac{R_a}{e_a} ; \quad (7)$$

The energy with the b vortices in the center is obtained by changing $a \rightarrow b$ and using $R_b^2 = N_b b^2$.

These expressions are valid when $r_{a,b} \ll a,b$, which means that the magnetic field should be sufficiently high, $H > H_c$, to compress the soft cores on the scale of the healing length of the spin-orbit coupling, $\eta \approx 10 \text{ m}$ [2]. In this approximation, the energies of the vortices of type a and b become equal when

$$\frac{a}{2} \frac{R^2}{a^2} \frac{p}{e} = \frac{b}{2} \frac{R^2}{b^2} \frac{p}{e} ;$$

If $a = 2 b = 2 \eta$, the rotation velocity for this is

$$= 2 \eta \frac{2}{2} \frac{p}{e} ; \quad (8)$$

The DQV becomes thus more favorable when $a > b$.

To explore the continuum approximation further, we minimize the energy in Eq. (6) for different situations:

(1) Full equilibrium, obtained after an adiabatic transition into the rotating superuid state. Here both R_a and the radius of the entire vortex cluster R_v are allowed to vary to minimize the free energy. If $b > a$, the radius R_a increases until it reaches R_v , so that only vortices of type a remain (see Eq. (6)). In the opposite case, R_a shrinks to zero, and only vortices of type b remain. The radius of the vortex cluster has its equilibrium value such that $d_{a(\text{eq})} = R_a = 2 \eta$ (or $d_{b(\text{eq})} = R_b = 2 \eta$, respectively), where $R_v = R_a = d_{(\text{eq})}$.

(2) Vortex numbers N_a and N_b are fixed: This case is realized when the entire vortex cluster has a radius R_v , which is smaller than that in the equilibrium state, so that vortices cannot annihilate at the container wall. From Eq. (5) we see that the radius of the vortex cluster is also fixed. The energy difference from Eq. (6) between the two configurations becomes

$$\frac{E(a;b) - E(b;a)}{E_0} = \frac{R_v^2}{R^2} \left(\frac{R_a^2}{R_v^2} - \frac{R_b^2}{R_v^2} \right) (b - a) = 0 ; \quad (9)$$

Thus the configurations (a;b) and (b;a) have the same energy, and the continuum approximation in the logarithm is limit it does not discriminate between them.

B. D iscrete vortex arrays

To identify structure-dependent contributions to the free energy we perform numerical calculations on discrete vortex arrays. Let us consider an array of N_j vortices with coordinates r_j , circulation's $\eta_j = \eta_j \eta_0$ with $j = 1, 2, \dots, N_j$ and the core radii η_j . The superuid velocity produced by vortices is

$$v_s = \sum_j \frac{X}{2} \frac{(r - r_j)}{|r - r_j|^2} \frac{(\eta - \eta_j^0)}{|r - r_j^0|^2} ; \quad (10)$$

The last term accounts for the image vortices with coordinates $r_j^0 = r_j R^2 / r_j^2$ reflected from the cylindrical surface for each true vortex located at r_j .

The interaction potential for vortices in a rotating superuid is equivalent to the Coulomb potential between charged lines immersed into a uniform background charge of opposite sign. The density of the background charge is proportional to η . The potential acting on each line is the sum of the potentials of the background charge, of the direct logarithmic Coulomb interaction, and the interaction with the wall reflection of each line.

The equations describing the dynamics of vortices are

$$\dot{r}_j = (1 - b^0) v_s^0 - b \dot{\eta}_j v_s^0 ; \quad (11)$$

where r_j is the velocity of j th vortex line, v_s^0 is the superuid velocity produced by all other vortices at the position of this reference vortex. The parameters b and b^0 are the reduced Hall-Vinen mutual friction parameters [12].

Fig. 1 shows a typical nalculation obtained in computer simulations of the growth of a bundle of SQV vortices. Vortices are created at the container wall and move under the action of the background potential of uniform rotation to the center of the container. This process is accomplished via large plastic deformations of the vortex bundle due to repulsive interactions with vortices already present in the container. The final structure of vortices in the central region can be considered as a hexagonal lattice with a large number of dislocations. Outer vortices form circular shells separated by a transition region from the central crystal.

The same calculations have been performed for two-component vortex arrays. Fig. 2 represents a simulation of a glassy vortex agglomerate, similar to the experimental situation shown in Fig. 11. The final state is shown, after DQV lines have been accumulated one by one from the same nucleation center into an existing cluster of SQV lines. Despite large plastic deformations in the bundle the DQV vortices form a compact drop. We observe neither periodical (chemical) structure nor any irregular structure of single DQV lines inside the SQV array.

To explain these results let us consider the energy of fixing for different periodical vortex structures with two

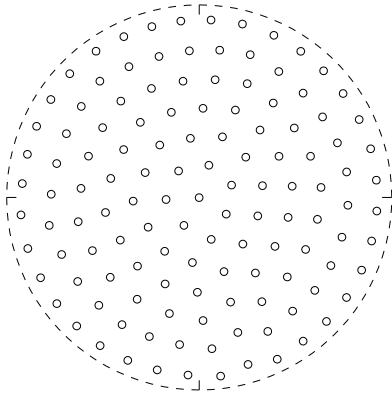


FIG. 1. Computer simulation of dynamics of SQ V vortices created one-by-one at the border of cylindrical container. The equations of motion (11) with $b^0 = 0$ are used. The final configuration of the array of $N_1 = 127$ vortices is shown. The dashed circle shows the border of a bundle $r = R_v$. Vortices in the center form a 2D hexagonal crystal with a large number of dislocations, whereas the outer vortices form a shell structure.

types of vortices in the elementary cell. Fig. 3 shows the difference between the free energy (per vortex line) of some periodical structures (up to 9 vortices per unit cell) and the sum of energies of two separate hexagonal crystals formed by SQ V and D Q V lines. These values have been obtained by using the planar summation method [13]. We see that for all these structures the energy of fixing is positive | the lowest energy corresponds two non-fixed lattices. These fact explain the tendency to form a compact drop of D Q V lines inserted into the SQ V array.

The equation of vortex motion (11) does not include any thermalization processes (annealing). Nevertheless, we expect that the resulting configurations of vortices are close to the optimal structure which provides a minimum of the free energy of the vortex array. We suppose that plastic deformations play an important role in relaxation to the energy minimum. Note that 2D Coulomb (logarithmic) interaction can be regarded as a soft-core potential in contrast to the hard-sphere approximation or to the Lennard-Jones system. This simplifies the relaxation of the vortex array to an optimal structure. Moreover, in contrast to 3D Coulomb systems where many crystal structures (bcc, fcc, hcp) have nearly the same total energy, the energy of a 2D hexagonal crystal is essentially lower than the energy of any other structure.

The results of the molecular-dynamics (MD) type of simulations of vortex array presented above correspond to the experiments where the rotation of a container with the superuid is being accelerated at a constant temperature kept below T_c . Cooling of the container through T_c at a constant produces a different situation. We expect that the final vortex configuration corresponds to

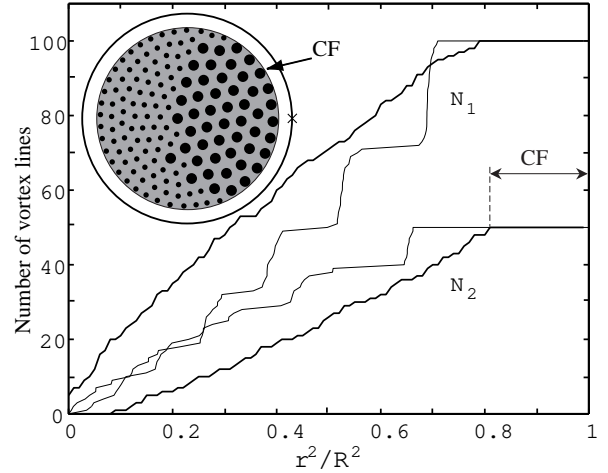


FIG. 2. Simulation calculation of an array with 100 SQ V and 50 D Q V lines. The D Q V lines have been accumulated one by one to an existing equilibrium array of SQ V lines, similar to the experiment in Fig. 11. The nucleation center, from where the D Q V lines are injected, is located on the cylindrical wall ($x = R$; $y = 0$) and is marked with a cross. The final configuration of the vortex agglomerate at 0.49 rad/s is shown in the inset. The total number of vortices corresponds to equilibrium circulation at 0.34 rad/s. The thin curves represent the radial locations of the SQ V and D Q V lines in the array: $N_i(r) = \sum_j (x_{ij}^2 + y_{ij}^2)^{1/2}$. They illustrate how the locations of the vortex lines concentrate more and more in concentric rings with increasing radius, although the nearest neighbor coordination is still triangular, as is visible from the inset. The thick curves correspond to deceleration records ($\dot{\phi} = 0.49$ rad/s! 0), similar to those measured in our experiment, and give the average radial distributions of $N_1(r^2)$ and $N_2(r^2)$.

the global minimum of the free energy. To check this we compare the free energies calculated for different vortex structures. First, it is necessary to modify the expression for the superuid velocity (10). We introduce the cutoff in the core region of the j th vortex such that we replace

$$\frac{r - r_j}{jr - r_j} \rightarrow \frac{r - r_j}{r^2(j)} ; \quad (12)$$

where $jr - r_j \gg (j)$ and $(j) \gg r_0$. Performing integration by part and neglecting all terms of the order $(r - r_0)^2$ we can rewrite Eq. (10) as

$$E = \sum_j \left[\frac{s_j^2}{4} \ln \frac{r_j^2 - R^2}{R(j)} + \frac{1}{4} + \frac{s_j}{2} (r_j^2 - R^2) \right] + \sum_{j \neq 1} \frac{s_j}{4} \ln \frac{jr_1 - r_j^2}{jr_1 - r_j R} ; \quad (13)$$

It is useful to introduce a vortex lattice energy which provides a more sensitive measure of the configuration dependent energy differences. Let us construct the same

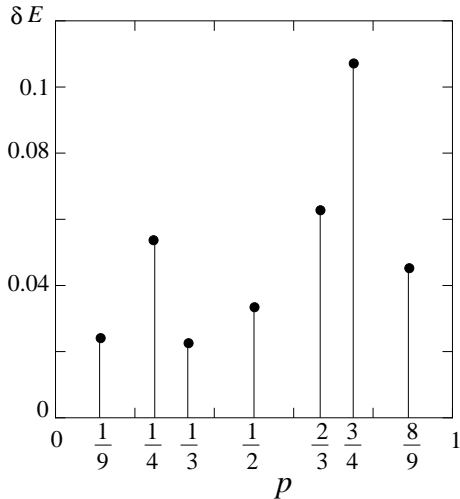


FIG. 3. The energy of fixing E for different periodical structures formed by SQV and DQV vortices. Zero level corresponds to the energy of two non-fixed hexagonal structures formed by the same vortices. The elementary cell includes n_1 SQV and n_2 DQV lines. The fractions near the points show the values of n_2 (numerator) and the total number of vortices in the cell $n_c = n_1 + n_2$ (denominator). The energy of fixing E is expressed in units of $s^2 = (2 n_c)$, $p = n_2/n_c$. The lattices with $n_c = 2$ and $n_c = 4$ have a square elementary cell, all other lattices are obtained by inserting of additional vortices into a hexagonal structure.

free energy as in Eq. (1) but with the super uid velocity written in the continuum approximation with $v_s = v_{s0}$, where v_{s0} is de ned by Eq. (3). The free energy in the continuum approximation is then [compare with Eq. (6)]

$$\begin{aligned} \tilde{E}^* f v_{s0} g &= \frac{s}{2} (v_{s0}^2 - 2v_{s0} v_{\text{rot}}) d^2 r \\ &= E_0 \frac{R_v}{R} \frac{4}{4} \frac{3}{4} \ln \frac{R_v}{R} \frac{R_v}{R}^2 : \end{aligned}$$

The difference of the two free energy expressions is the M adelung energy,

$$E_M = \tilde{E}^* f v_{s0} g - \tilde{E}^* f v_{s0} g ; \quad (14)$$

such that

$$E_M = \frac{s}{2} (v_s - v_{s0})^2 d^2 r : \quad (15)$$

The M adelung energy represents the vortex lattice contribution, it includes also the interactions with the image vortices. Within the logarithmic approximation it reduces to the second line of Eq. (6), and vanishes in the continuum approach.

Let us consider an array consisting of only one type (e.g. a) of vortices. We expect that the minimum energy at large N_a corresponds a con guration having an

ideal hexagonal structure in the center of the bundle, surrounded by a shell structure of outer vortices and an intermediate region between them. The average super uid velocity v_{s0} inside the vortex bundle is equal to the velocity of rotation (see Eq. (3)) and $v_s = v_{s0}$ in Eq. (15) is the super uid velocity measured in the rotating system. For an ideal periodic structure this velocity is also a periodic function of coordinates. The integration in (15) is reduced to the integration over a single W S cell.

$$E_M = N_a = \frac{s}{2} \int_{W S} (v_s - v_{s0})^2 d^2 r : \quad (16)$$

The area per vortex is $b_a^2 \frac{p}{3} = r_a^2$; it provides $b_a = 1.9046 r_a$ where b_a is the basis vector of W S cell for the type a vortices.

The periodic conditions require vanishing of the normal component of $v_s - v_{s0}$ at the border of each W S-cell. As a rst approximation we can replace the hexagonal W S cell by a cylindrical one with the same area. We refer to this approximation as the W S-cylinder. The super uid velocity (in the rotating coordinate frame) has only the azimuthal component and

$$j(v_s - v_{s0}) = \begin{cases} a r = (2 \frac{r}{a})^2; & \text{if } r < a \\ a = (2 r) & r; \text{ if } a < r < r_a. \end{cases} \quad (17)$$

The M adelung energy can be written as

$$E_M = N_a = \frac{s}{4} \frac{a^2}{a} \ln \frac{r_a}{a} : \quad (18)$$

where M will be referred as the M adelung constant. For the W S-cylinder approximation (17) $M = 1/2$. Comparing Eqs. (6) and (14) we obtain the relation between a in Eq. (7) and the M adelung energy: $a = (r_a = R)^2 [\ln(r_a = a) - M]$. This expression has been already used in Eqs. (6) and (7).

The M adelung constant M and the M adelung energy can be calculated exactly using the method of planar summation [13]. For an ideal hexagonal structure it yields

$$M = 0.49877. This value is extremely close to the value $M = 1/2$ obtained for the W S-cylinder approximation.$$

The M adelung energy for large but nite N_a can be written in the form

$$E_M = \frac{s}{2} \frac{1}{2} \left(\ln \frac{r_a}{a} - M \right) N_a + 2 R_v = b_a \quad (19)$$

Here the rst term in square brackets is the volume contribution, and the term proportional to a is the surface energy. The number of vortices in the outer vortex shell is $2 R_v = b_a$, where the intervortex distance b_a is supposed to be equal to the periodicity vector the ideal hexagonal structure: $b_a = 1.9046 r_a$.

To determine the surface energy we calculate E_M numerically for di erent values of N_a . To determine the vortex con guration corresponding the minimum of the

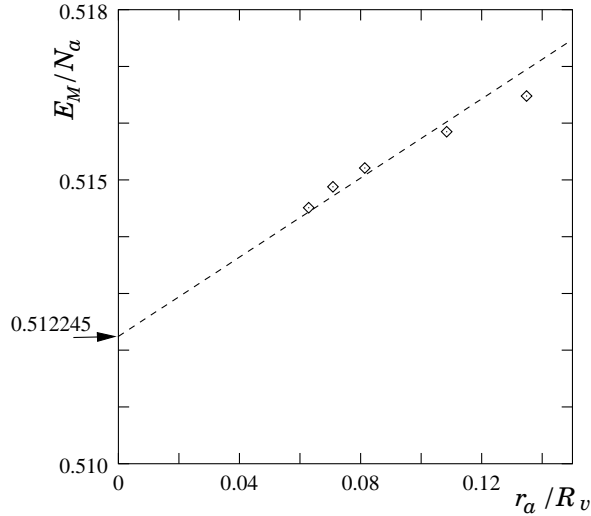


FIG. 4. The Madelung energy E_M for bundles of N_a vortices after many cycles of simulated annealing. $E_M = N_a$ (in units of $s_0^2 = 2N_a$) is plotted as a function of $r_a = R_v = N_a^{1/2}$ ($N_a = 55, 85, 151, 199, 253$). The container radius is fixed at $R = 40r_a$ and $a = r_a = 0.218$, which corresponds to SQV vortices with $a = 32$ m at $\omega = 0.5$ rad/s. The arrow left shows the value of $E_M = N_a = 0.512245$ obtained from Eq. (18) for an ideal hexagonal lattice (14). The dashed line presents the linear dependency (19) fitted to the results of computer simulations: $\omega = 0.0332$

free energy (13) we use the simulated annealing method already used in [3] to calculate the energy of large 3D ion clusters in ion traps. For the annealing, we consider the vortices as particles with a fictitious mass heated to some "temperature" which is modelled by a random force. The cooling is modelled by inserting a small viscous term in the Hamiltonian-like equations of motion. The heating-cooling cycles are introduced to allow the array to converge, as a function of time, to a minimum-energy configuration for a given number of vortices. For this configuration Eqs. (13) and (14) yield the free and the Madelung energies.

Fig. 4 shows the Madelung energy $E_M = N_a$ vs. $r_a = R_v = N_a^{1/2}$. We start from the ideal hexagonal lattice within the circle $r < R_v$. After many ($\sim 10^6$) heating-cooling cycles we arrive at the structure corresponding a minimum free energy (13). The results of this simulation show that the optimal structure of the vortex bundle is an ideal hexagonal structure in the center of the bundle surrounded by a quasi-shell structure near the surface with a transition region in between. Performing this procedure for different values of R_v we find the value of the $\omega = 0.0332$ in Eq. (19).

The same minimization procedure has been used for vortex array with two type of vortices. Fig. 5 shows

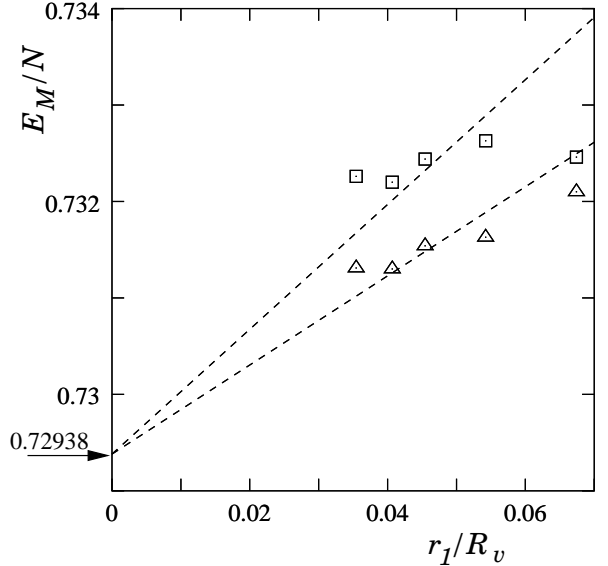


FIG. 5. Numerical minimization of the Madelung energy per circulation quantum, $E_M = N$, for two array configurations, as a function of the inverse of the normalized cluster radius: $r_1 = R_v = 1 = N$. E_M is expressed in units of $s_0^2 = 2$. The three configurations are compared at 5 cluster radii, when $N_1 = 2N_2 = N = 2$ and $N_2 = 55, 85, 121, 151, 199$. The parameters are $r_1 = r_2 = 0.2180$, $r_2 = r_1 = 0.3333$, which correspond to $r_1 = 32$ m and $r_2 = 49$ m at 0.5 rad/s. The container radius is fixed to $R = 40r_1 = 58$ m m.

the Madelung energy $E_M = N$ vs. $r_1 = R_v = N^{1/2}$, ($N = N_1 + 2N_2$). We have tested two possible vortex configurations: configuration (1) which corresponds to a cylindrical SQV bundle surrounded by DQV lines, and configuration (2) which is DQV bundle surrounded by SQV lines. We take $N_1 = 2N_2$ for both configurations. The interface between two types of vortices lies at $r = R_v = 2$. The results of computer simulations show that the optimal structure can be described as a nearly ideal hexagonal structure in a region far from both the outer surface and from the internal interface. Near the outer surface, a quasi-shell structure is established. The reconstructed interface demonstrates a complicated non-regular structure which is due to a contact of two hexagonal crystals with different periods: $b_2 = \sqrt{2}b_1$.

We see that the Madelung energy for configuration 2 is larger than for configuration 1. It can be attributed to a larger surface energy. Indeed, both configurations have the same number of vortices of each type and the same length of the interface between the two sorts of vortices. However, the outer shell for the configuration 2 is formed by the DQV lines. Since $r_2 = 2r_1$ and $r_2 = \sqrt{2}r_1$ one can see using Eq. (19) that the surface energy of DQV bundle is $\sqrt{2}$ times larger than the value for SQV lattice with the same value of R_v . These results show that the

minimum energy (for a given N_1 and N_2) corresponds to a hexagonal crystal of DQV vortices surrounded by SQV vortices.

IV. EXPERIMENTAL METHOD.

It turns out that the arrays, which we have explored, are naturally segregated due to the processes by which they are formed. We probe the structure of the vortex cluster with NMR measurement which records the average radial composition. The radial distributions of the two vortex species turn out to be different in the arrays produced by two different methods: An array with a common structure is not realized. In the first method of preparation the two types of lines are formed in the same transition to the superuid state on cooling through T_c in rotation, while in the second case they are created sequentially.

SQV and DQV lines each give rise to a satellite peak in the cw NMR spectrum, with characteristic frequency shifts different from each other and from the bulk liquid NMR line [14]. Both the peak height and the integrated intensity of the satellites are proportional to the total number N of vortex lines of the respective species and can be calibrated to give N . To measure the composition of a vortex cluster we monitor the peak height of a satellite as a function of the rotation velocity during slow deceleration, when the array expands and the outermost vortex lines annihilate one by one at the cylinder wall [15]. The peak height as a function of gives the number of the annihilating vortex lines as a function of r^2 . We can thus reconstruct the cumulative number of both types of vortices $N_1(r)$, together with their radial distributions $N_1(r)$, which they had prior to the deceleration from the original rotation velocity ω_0 . Here $N_1(r)$ is the number of vortex lines with quantum number inside a radius r . For reconstructing the radial distributions only one of the peak height dependences $N_1(r)$ needs to be measured. The requirement of solid-body rotation of the superuid component within the vortex bundle gives the relation: $N_1(r) + 2N_2(r) = 2r^2 = \omega_0$.

Measurements have been performed with two cylindrical containers, one fabricated from epoxy and the other from fused quartz [16]. Both are right circular cylinders 7 mm long and $R = 2.5$ mm in radius. They are closed off, except for an orifice of 0.5 mm in diameter, located in the center of the flat bottom plate. The orifice connects to a long tubular channel which provides via its liquid ^3He column the thermal contact to the refrigerator. The $^3\text{He-A}$ temperature in the container is determined from the calibrated temperature dependent frequency shift of the bulk liquid NMR absorption peak.

We may expect that a sufficiently slow cool down through T_c , one which approaches the adiabatic limit, will lead to an equilibrium state, where both the number

and the structure of vortex lines adjusts itself such that the total energy becomes minimized. This has been experimentally checked with respect to the number of lines when only one single species of vortex lines is present [15]. If two competing vortex species exist, for instance because of a transition between them as a function of ω , we expect that in a homogeneous superuid transition through T_c the rotating container will be filled with only one type of vortex lines, namely that structure which corresponds to minimum energy. Experimentally we find that there exist regions of coexistence around the various transitions of the vortex phase diagram [2], i.e. the vortex transitions have a width within which the two different species of lines are present simultaneously. Our interest here is to find out what types of inhomogeneity control the widths and what the configurations of the vortex arrays are in the coexistence regimes.

A. Results: dependence.

When the rotating sample is cooled in the NMR field through T_c , an equilibrium vortex state with only SQV lines is formed at low rotation, $\omega = 0.6$ [2]. Above this velocity also DQV lines are created. Their relative number increases with ω until above 3 rad/s no more SQV lines are observed. This coexistence regime in the transition from the SQV to the DQV structure as a function of ω is illustrated by the measurements in Fig. 6, where each data point (\circ) represents $\mathcal{I} = \mathcal{I}_{\text{tot}}$, the integrated NMR absorption I_v of the DQV satellite normalized to the total absorption I_{tot} in the NMR spectrum. The normalized absorption $I_v(\omega) = I_{\text{tot}}$ can be translated to vortex line numbers $N_2(\omega)$ by comparing to an equilibrium state with only DQV lines. The equilibrium number of type a vortex lines is given by

$$N_{\text{a(eq)}}(\omega) = (\mathcal{R} d_{\text{a(eq)}})^2 \frac{2}{\omega} / \frac{I_v(\omega)}{I_{\text{tot}}}; \quad (20)$$

where the width of the equilibrium CF annulus is $d_{\text{a(eq)}} = r_a [(1/2) \ln(r_a/a)]^{1/2}$ and the radius of the WS cell is given by Eq. (4). The calibration measurement, $N_{2(\text{eq})}(\omega)$, is plotted (\circ) in Fig. 6. In practice the equilibrium number of vortex lines is equal to that at the annihilation threshold [15], i.e. after deceleration when vortex lines have annihilated. In Fig. 6 the data for $N_{2(\text{eq})}(\omega)$ were measured by first increasing ω from zero to some high velocity $\omega > 3.5$ rad/s at $T = 0.81 T_c$ and by then decelerating sequentially to a lower value and recording there at constant ω the respective value of $I_v(\omega) = I_{\text{tot}}$. The difference between the two curves in Fig. 6 gives the number of SQV lines in the metastable coexistence regime: $N_1(\omega) = 2[N_{2(\text{eq})}(\omega) - N_2(\omega)]$.

There exists a critical rotation velocity ω_c which sets the region of coexistence for two types of vortices. According to Fig. 7 the value of ω_c lies within the interval

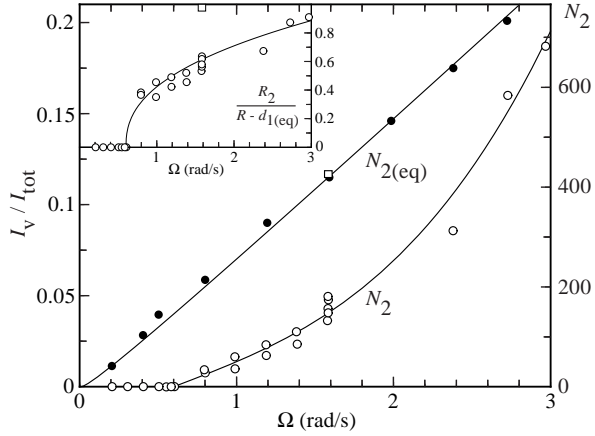


FIG. 6. Coexistence of SQ V and D Q V lines in the dipole-unlocked magnetic field regime ($H > H_c$), as a function of rotation velocity. (): Normalized D Q V satellite intensity $I_v = I_{\text{tot}}$ plotted as a function of the rotation velocity at which the sample was cooled through T_c . On the right vertical axis the intensity has been expressed in terms of line numbers, N_2 (), by means of the calibration, $N_2(\text{eq})$. At low Ω only SQ V lines are formed and $N_2(\Omega < 0.6 \text{ rad/s}) = 0$. Above 0.6 rad/s the coexistence regime starts, where the fraction of the total circulation in D Q V lines increases with Ω , until well above 3 rad/s no more SQ V lines are formed. As a guide for the eye, the solid curve represents $I_v = I_{\text{tot}} = 0.033(\Omega - 0.6) + 0.0084(\Omega - 0.6)^3$. The cool-down rate at T_c has been kept at $(dT = dt)_{T_c} = 5 \text{ K/m in}$, except for the data point marked with an open square (2), for which the cooling rate was $(dT = dt)_{T_c} = 18 \text{ K/m in}$. (): Calibration measurement of $I = I_{\text{tot}}$ with the equilibrium number of D Q V lines, $N_2(\text{eq})$. The fitted result gives $I_v(\Omega) = I_{\text{tot}} = 2.74 \cdot 10^4 N_2(\text{eq}) (\Omega - 0.0806) \frac{P}{(1 - 0.1 = \frac{P}{29.3})}$ (in rad/s). The inset shows the radius of the central D Q V cluster in relative units, together with a guide for the eye: $R_2 = (R - d_1(\text{eq})) = 0.618(\Omega - 0.6)^{0.41}$. Other conditions: $P = 29.3 \text{ bar}$, $H = 9.91 \text{ mT}$, the satellite intensities have been measured at $T = 0.81 T_c$.

0.6 to 3 rad/s. This can be compared with the theoretical prediction Eq. (8). A numerical estimate for R_2 can be derived from the normalized satellite intensity, which measures the effective dipole-unlocked soft-core area compared to that of the dipole-locked bulk liquid, or

$$\frac{I_v}{I_{\text{tot}}} = \frac{r_a^2}{r_0^2} = \frac{2}{2} \quad (21)$$

For the sake of comparison, the best values for the satellite intensities come from measurements at $0.50 T_c$ (11.7 mT, and 33.9 bar): In the equilibrium state the proportionality factor in front of I_v in Eq. (21) was found to be 0.094 for SQ V lines and 0.114 for D Q V lines. These give for the soft core radii $r_1 = 32 \text{ m}$ and $r_2 = 49 \text{ m}$, which appear to be reasonable estimates. From the con-

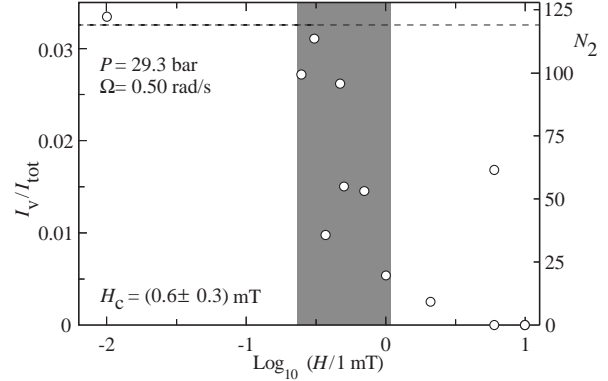


FIG. 7. Coexistence of SQ V and D Q V lines as a function of magnetic field H below 0.6 rad/s : Normalized D Q V satellite intensity $I_v = I_{\text{tot}}$ plotted vs the field H , which was applied during cooling through T_c at 0.5 rad/s . On the right vertical axis the NMR absorption intensity has been converted to vortex numbers, $N_2(H)$, using the calibration in Fig. 6. The horizontal dashed line represents the equilibrium number, $N_2(\text{eq})$, for dipole-unlocked D Q V lines. The shaded region marks the width of the coexistence regime around the critical field, $H_c = 0.6 \text{ mT}$. In this measurement the field was increased to the NMR value 9.91 mT below the superuid transition, while the sample was cooled to $0.81 T_c$, where the intensity $I_v = I_{\text{tot}}$ was measured. Other conditions were the same as in Fig. 6. Thus after a superuid transition at $H < H_c$ and a subsequent increase of the field to its NMR value above H_c , approximately the equilibrium number of D Q V vortices is obtained. When the field $H > H_c$, $N_2 \approx 0$ in accordance with the results in Fig. 6.

tinuum approximation result in Eq. (8) we now get for the transition from SQ V to D Q V lines $\approx 14 \text{ rad/s}$. This estimate is based on the differences in quantization number and core size, and the crude approximation for the vortex energy in Eq. (7). 14 rad/s is an order of magnitude more than the measurements in Fig. 6 suggest.

B. Magnetic field dependence.

In addition to Ω , the second important variable is the magnetic field H [17] in the vortex phase diagram: At high field in the regime of the NMR measurements, the SQ V and D Q V are in the form of well-separated vortex lines, with $r_a \ll r_0$. As before, r_a is the radius of the soft vortex core where the \hat{d} and \hat{l} fields are dipole unlocked. At low field the \hat{d} and \hat{l} fields are dipole locked everywhere, also within the soft vortex core, which now has a large radius $r_a \approx r_0$. In this regime the singular SQ V is not stable. In the transverse plane (?) the dominant vortex texture appears to be a square lattice, consisting of a unit cell with four quanta of circulation [2,6].

The transition between the low and high field regimes as a function of H is illustrated by the measurements in Fig. 7 at a low value of Ω . Our NMR measurements are performed at a fixed frequency in the high field limit. Therefore they have to follow a particular routine. First, the container is cooled through T_c at constant Ω , with the field adjusted to the value given on the horizontal axis. Next, below T_c the field is increased to the NMR value of 9.91 mT. During the field sweep the low field vortex texture transforms to its high-field dipole-unlocked counterpart, with well-separated vortex lines. Here the square lattice with singularity-free vorticity is changed into DQV lines while any vortices with a singular hard core remain singly quantized. At high temperatures ($T > 0.8 T_c$) the dipole-unlocking transition occurs easily within the soft cores while at low temperatures ($T < 0.6 T_c$) dipole locking survives in a metastable form and a high-field "quasi-dipole-locked variant" of the DQV soft core is formed [14]. Finally, the container is cooled to 0.81 T_c , and the DQV satellite intensity is measured.

As shown in Fig. 7, we find a critical field $H_c = 0.6$ mT. Above H_c the SQV lines dominate, as required when $\Omega < 0.6$ rad/s. Below H_c DQV lines are found, which are obtained from the singularity-free low-field vortex textures. Centered around H_c there is a coexistence regime with a width of 0.5 mT, where both types of vortex lines are present.

On comparing Figs. 7 and 8 it is noted that both the critical field and the width of the metastable regime increase with the rotation velocity at which the container is cooled below T_c [2]. In the case of Fig. 8 both the DQV and SQV satellite intensities were determined separately. On the low field side only DQV lines are found. On the high field side both types of lines are formed, with a 4 times larger share of the total circulation carried by the SQV lines. This is the same ratio as was already seen in Fig. 6 at 1 rad/s.

In a magnetic field the superfluid transition splits into T_{c1} from the normal to the A_1 phase and into T_{c2} from A_1 to the A_2 phase (the latter is the regular $^3\text{He}-\text{A}$). The thermal width of the A_1 region is narrow, approximately 0.6 K at 10 mT. What effect does the intermediate A_1 phase have on the DQV to SQV ratio? A more change to be expected at fields much larger than those shown in Figs. 7 and 8? We find that at least a cooldown in 60 mT field at 1.4 rad/s gives the same result as at 10 mT.

C. Cooling rate dependence.

Surprisingly, in Fig. 6 one data point deviated from the typical behavior (denoted with (2) at 1.6 rad/s). The only distinction that could be appended to this measurement, compared to others at the same rotation velocity, was a larger cooling rate during the superfluid transition: The five data points measured at cooling rates

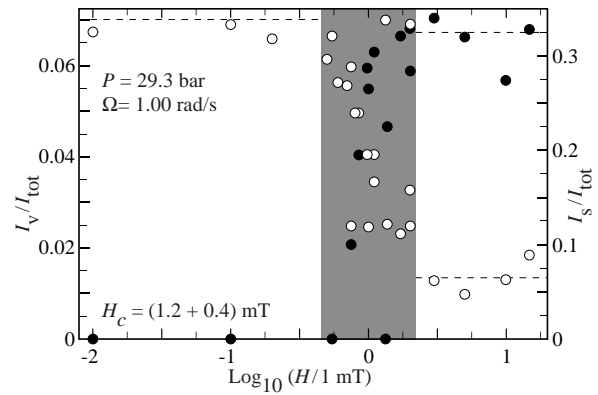


FIG. 8. Coexistence of SQV and DQV lines as a function of magnetic field above 0.6 rad/s: The normalized intensities $I_v = I_{\text{tot}}$ of the DQV satellite (●; left vertical axis) and $I_s = I_{\text{tot}}$ of the SQV satellite (○; right vertical axis) have been plotted as a function of the magnetic field H , which was applied during cooling through T_c at 1 rad/s. The horizontal dashed line on the left represents the equilibrium value expected for DQV lines, after a superfluid transition at low fields ($H < H_c$) and a subsequent increase of the field to 9.91 mT. On the right ($H > H_c$), the dashed lines give the mean values for the SQV and DQV lines: $N_1 = 440$ and $N_2 = 48$. The shaded region marks the width of the transition regime around the critical field, $H_c = 1.2$ mT. The coexistence regime includes both the shaded and the high field regions, $H > H_c$. The same conditions apply as in Fig. 6, including the calibration for the DQV satellite intensity. The calibration for the SQV satellite intensity is $N_{1(\text{eq})} () / I_{\text{tot}} = 0.43 (1 - 0.089 = \frac{1}{P})$ (in rad/s).

$\frac{dT}{dt} = \frac{1}{5} \text{ K/m in}$ gave for the relative amount of DQV lines $N_2 = N_{2(\text{eq})} = 0.38$ while the anomalous point at a cooling rate of 18.5 K/m in fell on the equilibrium result $N_{2(\text{eq})}$, with no SQV lines detected at all.

Additional evidence is shown in Fig. 9 on how an increasing cooling rate at T_c shifts vorticity from the SQV to the DQV lines. Here a fused quartz sample container was used in which $^3\text{He}-\text{A}$ could be supercooled to below 0.49 T_c . At lower temperatures the measuring resolution is improved due to the larger frequency shifts separating the NMR lines from each other [14]. When the cooling rate in Fig. 9 at 1.4 rad/s reaches 5 K/m in a changeover takes place from SQ to DQV lines: at lower rates only one fourth of the total circulation is in DQV lines (which is the same fraction as in Fig. 6), while above 6 K/m in, only few SQV lines are formed. Similar measurements at 0.6 rad/s with cooling rates up to 16 K/m in did not yet produce a DQV satellite of measurable height.

Later measurements with a new cylindrical quartz container, which was connected with a still smaller channel of less than 0.4 mm diameter to the heat exchanger, did

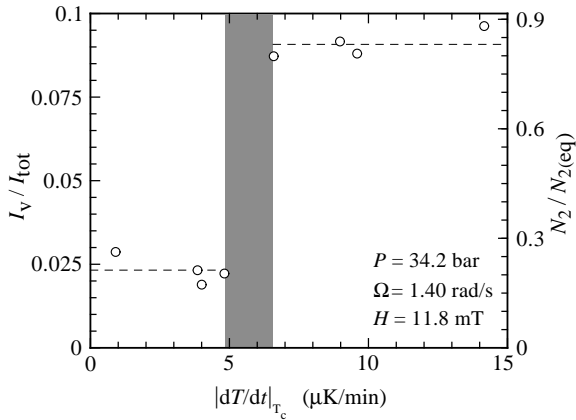


FIG. 9. Influence of the cooling rate at T_c on the relative amount of SQV and DQV lines: Normalized DQV satellite intensity I_v/I_{tot} plotted as a function of cooling rate during the transition through T_c at 1.4 rad/s. The right vertical axis gives the fraction of the total circulation in DQV lines while the rest, $1 - N_2/N_{2(\text{eq})}$, is carried by SQV lines. The satellite intensities were measured at $(0.49 \pm 0.51) T_c$, where the calibration for the primary DQV line satellite is $N_{2(\text{eq})} () / I_v () = I_{\text{tot}} = 0.078 (1 \pm 0.11) \text{ (in rad/s)}$.

not display SQV lines in any situation. The smaller channel size increases the thermal resistance to the container and leads to rapid irreversible norm al-to-superuid transitions, where the transition velocity cannot reliably be controlled externally. This suggests that a large cooling rate and nonequilibrium conditions enhance the formation of DQV lines and may prevent SQV lines from being created altogether.

There is one data point also in Fig. 7 at 6 mT with a larger fraction of DQV lines than what one would expect on the basis of the general behavior. In the measurements as a function ofeld (Figs. 7 and 8) the cooling rate at T_c cannot be monitored accurately, since the NMR measurement is inoperative at that stage. Therefore a cooling routine was worked out which should have yielded rates of less than 5 K/min. In the case of the anomalous data point in Fig. 7 either a mistake occurred in the application of the cooling routine or one more variable exists which affects the DQV to SQV ratio and is not identified by our measurements.

D. Spatial distribution of coexisting vortices.

In Fig. 10 the radial composition of an array is shown which has been created by cooling through T_c at 1 rad/s. Here the distributions of the two vortex species are segregated: The SQV lines annihilate first and the DQV lines later. This behavior corresponds to the concentric array

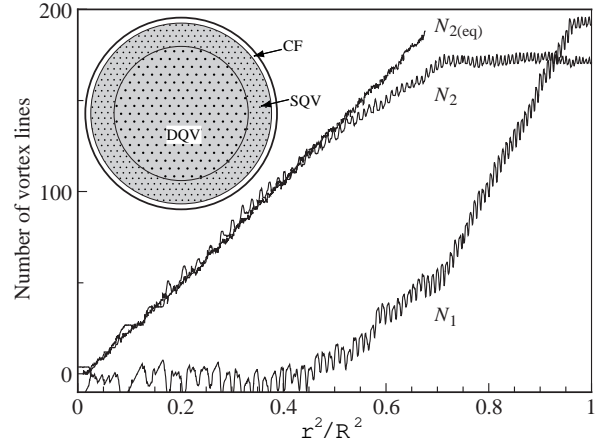


FIG. 10. Radial distributions $N_1(r^2)$ and $N_2(r^2)$ after cooling through T_c at 1 rad/s and 1.1 mT. The deceleration from 1 rad/s to zero is performed at 0.81 T_c and 9.91 mT. Other conditions are the same as in Fig. 11. $N_{2(\text{eq})}$ shows for comparison the deceleration for an array consisting of only DQV lines. It is prepared by cooling through T_c at > 1.5 rad/s in zero field and by then sweeping the field up to 9.91 mT at 0.81 T_c . The final part of the deceleration below 0.7 rad/s is shown here. As demonstrated in Ref. [15], during such a deceleration (at $d = dt = 1.5 \times 10^3 \text{ rad/s}^2$) the total circulation at any value of r corresponds roughly to that in the equilibrium state. The inset illustrates schematically a transverse cross section through the rotating container with the coaxial array configuration: the SQV lines (small dots) are in the outer annulus and the DQV lines (large dots) in the center.

structure, shown in the inset of Fig. 10, which consists of a central region of 130 DQV lines, a peripheral annulus of 140 SQV lines, and the exterior vortex-free CF region of equilibrium width. The boundary between the DQV and SQV regions is relatively sharp (10% of the radius of the array, or additionally roughly 40 DQV and 50 SQV lines).

No noticeable change in the coaxial configuration is observed from the noise in the rotation drive ($j = 1 \pm 10^3 \text{ rad/s}$), when the same array is monitored for several hours in stable conditions, or while the externally controllable parameters are varied, e.g. if modulated sinusoidally (without decreasing or increasing the number of lines). This suggests that any spontaneous reordering of the two vortex species into a mixed array is below our measuring resolution.

The segregation into two coaxial domains, with the SQV lines in the outer annulus of the vortex cluster, is always observed when both vortex species are found to coexist after cooling through T_c . We also find, by measuring the width of the CF annulus [15], that the total number of lines adjusts itself so that the energy is minimized. This is expected, since the total circulation cor-

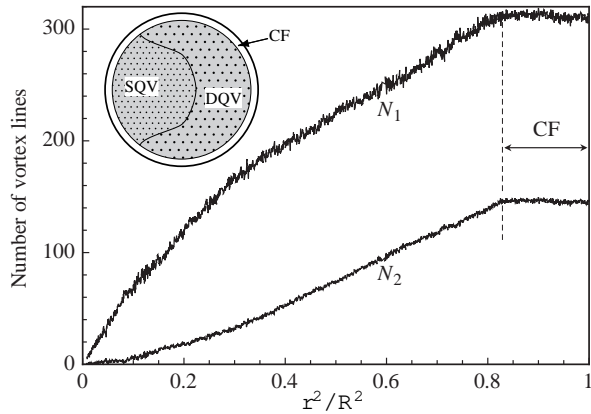


FIG. 11. Radial distributions $N_1(r^2)$ and $N_2(r^2)$ in an array, which originally was an equilibrium state of SQV lines, but to which DQV lines were added later. The SQV array was prepared at 29.3 bar pressure and 9.91 mT field, by cooling through T_c at 7 K/m in and 0.6 rad/s. The cooling was then continued until 0.81 T_c , where was slowly increased to 1.4 rad/s, to create the DQV lines. The final step was a slow deceleration to zero, during which the radial vortex line distributions were recorded. The velocity sweeps were performed at $\Delta t = dtj = 2 \times 10^3$ rad/s². The critical CF velocity of vortex formation at 1.4 rad/s was $v_c = 0.24$ rad/s, which corresponds to a linear velocity of $v_c = 0.60$ mm/s. The inset illustrates schematically the array configuration, a plastically deformed agglomerate of vortex lines.

responds to a dominant energy term, while the structure of the vortex line, in the metastable region close to a transition between two competing species, is controlled by energy contributions which are orders of magnitude smaller.

E. Plastic deformation of vortex array.

Coeexistence of the two vortex species can also be artificially arranged, by making use of their metastability. We use the following procedure: The sample is first cooled through T_c at 0.6 rad/s and $H > H_c$, so that an equilibrium vortex state with only SQV lines is formed. DQV lines are added later, by increasing slowly while the temperature is already below T_c , such that the desired number of DQV lines is created at a stable critical counterflow velocity v_c [1]. In this case the DQV lines are injected one at a time to the existing array, presumably from the same nucleation center on the cylindrical wall where the superflow instability takes place (i.e. they are thought to emanate from a rectilinear source which is close to the cylindrical wall and parallel to the rotation axis [1]).

In Fig. 11 the radial decomposition of an array is shown which has been prepared with this procedure, by adding

150 DQV lines to an existing equilibrium array of 310 SQV lines. During deceleration, initially both types of vortices are seen to annihilate, but on moving closer to the center the proportion of DQV lines is reduced and the SQV lines start to dominate. Such an annihilation record could correspond to the configuration shown schematically in the inset of Fig. 11, which in turn could result from the process by which the array was formed.

The DQV lines are here formed in a regular periodic process, where a newly created DQV line arrives roughly to the same spot at the edge of the array. It makes space for itself by pushing the existing lines aside. In this way the DQV lines end up residing in a segregated pocket at the edge of the cluster, if no mixing of lines occurs later. From the data in Fig. 11 it is not possible to judge how sharp the boundary of this pocket is and to what extent mixing of the two vortex species might have occurred. However, no significant change from this configuration is noticed even if the cluster is subjected to rapid modulation of the rotation velocity with an amplitude which does not yet add new vortices or annihilate existing ones. On this basis we expect spontaneous reordering or annealing in the array to be unimportant and that it resembles a random agglomerate with much reduced long range order.

F. Homogeneity of superfluid transition.

In any real experiment the superfluid transition is expected to acquire some degree of inhomogeneity and irreversibility. In the present case the main source is the thermal resistance concentrated in the orifice of the container. The liquid ³He column consists of the heat exchanger volume on the bottom in contact with the refrigerator and the sample container on the top at the end of a long tube [16]. During cooldown a thermal gradient is present, in addition to the residual heat leaks, which keep the top end of the container as the warmest point in the ³He column. This means that the heat flow through the orifice is composed of the cooling rate of the liquid and the residual heating leaking out from the walls of the rotating container. At a cooling rate of 1 K/m in the heat flow from the container is of order 0.5 nW and the thermal gradient inside the container 0.5 K/mm (at $T_c = 2.4$ mK).

The superfluid transition emerges as a transition front through the orifice on the bottom of the cylinder. Initially it adopts a hemispherical shape [9]. The width of the phase front is determined by the local thermal gradient and thermal fluctuations. Its velocity can be controlled externally by adjusting the cooling rate. Simultaneously the heat flow is carried by a superfluid thermal countercurrent, which appears below T_c and converges towards the orifice. It is oriented dominantly in the axial direction, transverse to the rotational flow.

In equilibrium conditions at low the SQ V is the minimum energy vortex structure, but thermal CFC or other inhomogeneities in an irreversible nonequilibrium transition provide a bias for DQV lines to be formed. This perturbation is concentrated in the neighborhood of the origin, from where vortex formation starts during the superuid transition. Here DQV lines are created first and SQV lines appear later when the transition front expands into the more homogeneous peripheral region of the cylinder. This interpretation is suggested by the strong dependence on the cooling rate at T_c .

V. CONCLUSION

We have focused on two questions: (1) the configuration of the vortex array in the coexistence regime and (2) the metastability and width of the SQV \rightarrow DQV transition. By comparing experiment to numerical simulation, we conclude that below T_c vortex arrays are formed by plastic deformation: Vortex lines are frozen in the array to the configuration in which the array was formed. High energy barriers separate different array configurations and thermally activated processes (or any other mechanism) are not able to anneal faults to a new structure with lower energy and better long range order.

In arrays formed by cooling through T_c in rotation, a coaxial configuration is observed, with the SQV lines located in the outer annular region. The phase boundary in Fig. 9 suggests that the cooling rate at T_c is one of the controlling factors for the formation of DQV lines: At low SQV lines are formed in the equilibrium situation while nonequilibrium conditions favor the formation of DQV lines. In the experiment, axially oriented heat flow converges towards the origin, located in the center of the bottom plate of the rotating container. SQV lines are then more readily formed in the outer parts of the container which are closer to equilibrium. Thus the boundary between the two coaxial domains becomes a similar phase boundary as that shown in Fig. 9, but now as a function of the radial coordinate r of the container, along which the cooling rate varies as the normal-to-superuid phase front moves through the cylinder.

From our numerical analysis on arrays with discrete vortex lines we find that the peculiar coaxial configuration, with the SQV lines in the outer annular region, is energetically preferable over the opposite configuration, by roughly 3–10% of the Madelung energy per circulation quantum. This small energy gain, which takes place on the scale of the intervortex distance rather than the container dimensions, is a result from the reduced surface energy in a cluster with the vortex lines of lower quantum number located at the outer interface.

This work was funded by the EU Human Capital and Mobility Programme (grants CHGECT 94-0069 and ERBFMGECT 980122) and by INTAS (grant 96-0610).

NBK acknowledges support from the Russian Foundation for Basic Research (grant 99-02-16043).

- [1] V. Ruutu, J. Kopus, M. Korusius, U. Parts, B. Placais, E. Thuneberg, and W. Xu, *Phys. Rev. Lett.* **79**, 5058 (1997).
- [2] U. Parts, J.M. Karimaki, J.H. Koivunen, M. Korusius, V.M. Ruutu, E.V. Thuneberg, and G.E. Volovik, *Phys. Rev. Lett.* **75**, 3320 (1995).
- [3] R.W. Hasse and V.V. Avilov, *Phys. Rev. B* **44**, 4506 (1991).
- [4] D. Vollhardt and P.W. Olle, *The Superuid Phases of Helium 3* (Taylor & Francis, London, 1990).
- [5] H.K. Seppala, P.J. Hakonen, M. Korusius, T. Ohmura, M.M. Salomaa, J.T. Simola, and G.E. Volovik, *Phys. Rev. Lett.* **52**, 1802 (1984).
- [6] E.V. Thuneberg and J.M. Karimaki, *Physica B* **194**–**196**, 777 (1994); *Phys. Rev. B*, in press.
- [7] A.L. Fetter, in *Progress in Low Temperature Physics*, ed. D.F. Brewer (North-Holland, Amsterdam, 1986), Vol. 10, p. 1; M.M. Salomaa, and G.E. Volovik, *Rev. Mod. Phys.* **59**, 533 (1987).
- [8] H.K. Seppala and G.E. Volovik, *J. Low Temp. Phys.* **51**, 279 (1983); V.Z. Vulovic, D.L. Stein, and A.L. Fetter, *Phys. Rev. B* **29**, 6090 (1984).
- [9] M. Korusius, E.V. Thuneberg, and U. Parts, *Physica B* **197**, 376 (1994).
- [10] L.J. Campbell and R.M. Zi, *Phys. Rev. B* **20**, 1886 (1979).
- [11] I.M. Khalatnikov, *An Introduction to The Theory of Superuidity* (W.A. Benjamin Inc., New York, 1965).
- [12] T.D. Bevan, A.J.M.anninen, J.B. Cook, H. Alles, J.R. Hook, and H.E. Hall, *J. Low Temp. Phys.* **109**, 423 (1997); *Phys. Rev. Lett.* **77**, 5086 (1996).
- [13] V.V. Avilov, *Solid State Commun.* **44**, 555 (1982).
- [14] V.M. Ruutu, U. Parts, and M. Korusius, *J. Low Temp. Phys.* **103**, 1 (1996).
- [15] V.M. Ruutu, J.J. Ruohio, M. Korusius, B. Placais, E.B. Sonin, and W. Xu, *Phys. Rev. B* **56**, 14089 (1997); *Physica B* **255**, 27 (1998).
- [16] V.M. Ruutu, U. Parts, J.H. Koivunen, N.B. Koprin, and M. Korusius, *J. Low Temp. Phys.* **107**, 93 (1997).
- [17] J.P. Pekola, K. Torizuka, A.J.M.anninen, J.M. Kyynäräinen, and G.E. Volovik, *Phys. Rev. Lett.* **65**, 3293 (1990).